

## Mid-rapidity $\phi$ meson production at $\sqrt{s_{NN}} = 200$ GeV Au+Au and pp collisions from STAR

Jingguo Ma<sup>1,a</sup> for the STAR Collaboration

<sup>1</sup> University of California, Los Angeles,  
90095 Los Angeles, USA

**Abstract.** We present the results for the measurement of  $\phi$  meson production in  $\sqrt{s_{NN}} = 200$  GeV Au+Au and pp collisions at the Relativistic Heavy Ion Collider (RHIC). Using the event mixing technique, spectra and yields are obtained from the  $\phi \rightarrow K^+K^-$  decay channel for five centrality bins in Au+Au collisions and in pp collisions. We observe that the spectrum shape in Au+Au collisions depends weakly on the centrality and the shape of the spectrum in pp collisions is significantly different from that in Au+Au collisions.

*Keywords:* Relativistic Heavy Ion Collisions,  $\phi$ , Meson

*PACS:* 25.75.Dw

### 1. Introduction

Strangeness production in Relativistic Heavy Ion Collisions may provide detailed information on the collision dynamics [ 1]. The enhanced production of strangeness in nucleus-nucleus collisions is predicted to be a signature that the collisions go through a deconfined stage - namely the quark gluon plasma (QGP) [ 2, 3]. The  $s\bar{s}$  quark content for the  $\phi$  meson is of particular interest: The production of  $\phi$  meson may be sensitive to strangeness enhancement [ 2, 3, 4]. The possible mass and decay width modification of  $\phi$  meson due to the expected partial chiral symmetry restoration and in medium effect in the hot and dense matter has been a topic of both theoretical and experimental investigations [ 5, 6, 7, 8, 9]. The  $\phi$  meson may retain the information from the early partonic stage of the collisions since it is expected that  $\phi$  meson interacts weakly with nonstrange hadrons during the hadronic stage [ 3, 4]. Finally, the comparison of the production of  $\phi$  meson in Au+Au and pp collisions at the same beam energy may yield knowledge on the production mechanisms of  $\phi$  meson and the evolution dynamics of the colliding system.

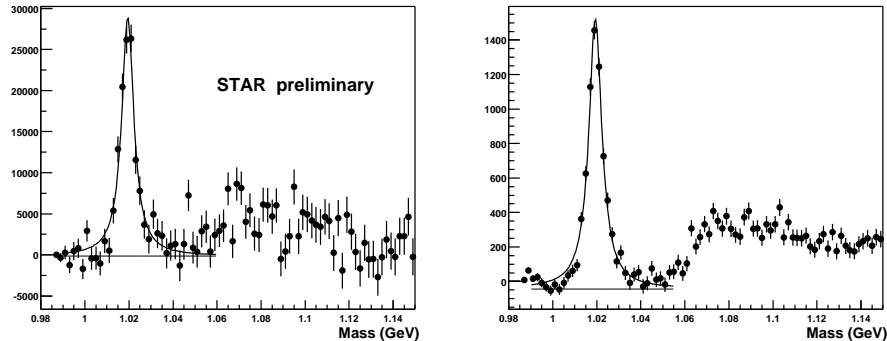


**Fig. 1.** Background subtracted  $K^+K^-$  pair invariant mass distribution from the top 10% central Au+Au collisions (left panel) and pp collisions (right panel). The  $\phi$  peak is fitted to a Breit-Wigner function plus a linear background function representing the background. The residual background at higher mass region comes from misidentified  $K_s^0$  decay products.

## 2. Experiment and Data Analysis

The results on  $\phi$  meson production at  $\sqrt{s_{NN}} = 130$  GeV from the STAR detector have been reported [10]. The data presented here was taken by the STAR detector [11] during the second run of RHIC collider in the year 2001. The main components of the STAR detector used in this analysis are a large acceptance Time Projection Chamber (TPC) [12], a Central Trigger Barrel (CTB) and two Zero Degree Calorimeters. The TPC is placed in an uniform magnetic field as the tracking device for charged particles. The CTB and ZDC are used for triggering. In this analysis about 2.1M events from minimum bias trigger data and 0.5M events from central trigger data in Au+Au collisions and 4M events from minimum bias trigger data in pp collisions are used after all event selection cuts [10].

The particle identification is achieved by correlating the measured energy loss ( $dE/dx$ ) of the particle in the TPC gas with its momentum. In this analysis, a track is selected as a kaon candidate as long as its  $dE/dx$  is within  $2\sigma$  of the kaon Bethe-Bloch curve. Due to limited resolution of the detector, the pion and kaon  $dE/dx$  bands merge at momentum greater than 0.7 GeV, resulting in the pion contamination in the kaon candidates. The centrality in Au+Au collisions is defined by the fraction of the total inelastic hadronic cross-section, i.e. by dividing the raw charged hadron multiplicity distribution into centrality classes. For the  $\phi$  analysis, the centrality division for the Au+Au collisions is: top 5% from central trigger data and top 10%, 10-30%, 30-50%, 50-80% from minimum bias trigger data.

The  $\phi$  signal is built by calculating the invariant mass of every selected  $K^+K^-$  pair. The shape of the combinatorial background is calculated by event mixing technique [13, 14]. For the Au+Au data analysis, each event is mixed with another event in the same centrality class, while each event is mixed with four other events

in the pp data analysis in order to get a better description of the background with higher statistics.

### 3. Results

The background subtracted  $K^+K^-$  pair invariant mass distribution averaged over  $0.4 \text{ GeV}/c \leq p_T \leq 3.9 \text{ GeV}/c$  is shown in fig. 1. The  $\phi$  peak is fit to a Breit-Wigner function plus a linear function representing the background in each  $p_T$  bin. The measured mass for the  $\phi$  meson in both Au+Au and pp collisions is  $1019 \pm 0.7 \text{ MeV}/c^2$ , which is consistent with the  $\phi$  meson mass from the Particle Data Group [ 15]. The measured width is also consistent with the  $\phi$  natural width convoluted with the resolution of the STAR detector. The residual background at mass region greater than  $1.06 \text{ GeV}/c^2$  mainly comes from  $K_s^0$  decay products when pions are misidentified as kaons. A small fraction of it may also come from  $\Lambda$  decays where both of its decay daughters are misidentified as kaons.

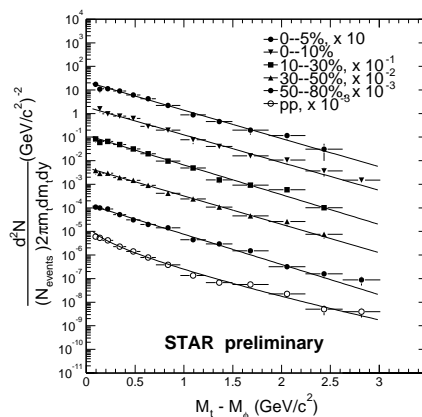


**Fig. 2.**  $\phi$  invariant multiplicity distribution as a function of transverse mass for five centrality bins in Au+Au collisions (filled symbols) and pp collisions (open symbols) at  $\sqrt{s_{NN}} = 200$  GeV. The spectra are scaled by different factors to guide eyes.

In order to obtain the resonance yield, detector acceptance and efficiency corrections were applied to the uncorrected number of  $\phi$  for each centrality and  $p_T$  bin. The acceptance and efficiency corrections were done by embedding simulated kaons from  $\phi$  decays into real events using GEANT, and by passing them through the full reconstruction chain [ 10, 16]. The corrected  $\phi$  invariant multiplicity distributions at mid-rapidity ( $|y| < 0.5$ ) as a function of  $m_T - m_\phi$  are depicted in Fig. 2, where  $m_\phi = 1019.4 \text{ MeV}/c^2$  is the average  $\phi$  mass reported in [ 15]. The transverse momentum coverage for this measurement is  $0.4 \leq p_T \leq 3.9 \text{ GeV}/c$ , which corresponds to 85% of the  $\phi$  yield at mid-rapidity. In Au+Au collisions, the spectra are fitted by an exponential function in  $m_T - m_\phi$  for all centrality bins. In pp collisions, the

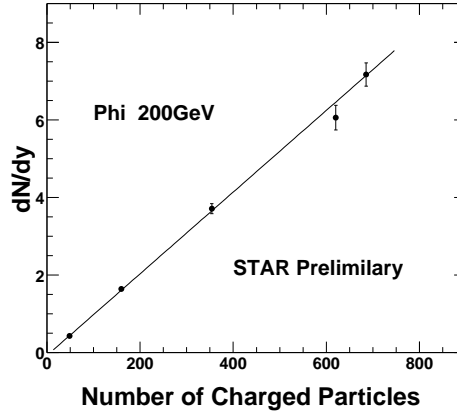


**Fig. 3.**  $\phi$   $dN/dy$  as a function of number of charged particles for Au+Au collisions.  $dN/dy$  of  $\phi$  scales linearly with number of charged particles in Au+Au collisions.

spectrum is better represented by a power law function in  $p_T$ . Thus the spectra shape changes from pp to Au+Au collisions. In Au+Au collisions, the inverse slopes extracted from the exponential function fit to the spectra do not depend strongly on the collision centrality.

The  $\phi$  yield ( $dN/dy$ ) obtained from the fit to the spectra in Au+Au collisions as a function of the number of charged particles is shown in Fig. 3. The number of charged particles corresponds to the acceptance and tracking efficiency corrected charged particle multiplicity within  $|\eta| < 0.5$ , where  $\eta$  is the pseudorapidity. The measured  $\phi$  yield scales linearly with the number of charged particles produced in Au+Au collisions.

The  $\phi < p_T >$  calculated from the fits to the spectra as a function of the number of charged particles is depicted in Fig. 4, where the solid triangle and the solid circles sketch the measurements in pp and Au+Au collisions, respectively. In this figure, the  $< p_T >$  of  $\pi^-$ ,  $K^-$  and  $\bar{p}$  from [17] are also plotted, where the open triangles represent the  $< p_T >$  obtained in pp interactions and the open circles correspond to the  $< p_T >$  measured in Au+Au collisions for different centralities. The  $< p_T >$  of  $\pi^-$ ,  $K^-$  and  $\bar{p}$  increases from peripheral to central collisions and from lighter to heavier particles. The  $\pi^- < p_T >$  increase from pp and most peripheral Au+Au collisions to the most central Au+Au collisions is about 10%. In the case of  $K^-$  and  $\bar{p}$ , the increase is about 25% and 60%, respectively. This behavior is expected from collective flow with hadronic rescattering. The  $\phi$  meson has a very different behavior: Its  $< p_T >$  increases from pp collisions to Au+Au collisions. However, there is little increase from peripheral Au+Au to central Au+Au collisions although its mass is even higher than that of  $\bar{p}$ . Some hadronic hydrodynamic calculations [

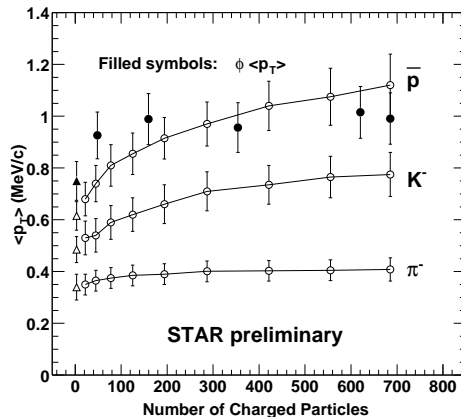


**Fig. 4.** The  $\langle p_T \rangle$  of  $\phi$ ,  $\pi^-$ ,  $K^-$  and  $\bar{p}$  at  $\sqrt{s_{NN}} = 200$  GeV Au+Au and pp collisions as a function of the number of charged particles. The triangles represent the  $\langle p_T \rangle$  obtained in pp interactions and the circles correspond to the  $\langle p_T \rangle$  measured in Au+Au collisions for different centralities.  $\phi \langle p_T \rangle$  in pp collisions is extracted from power law  $p_T$  fit function. In Au+Au collisions,  $\phi \langle p_T \rangle$  is extracted from exponential  $m_T$  fit function.  $\phi \langle p_T \rangle$  shows a very different behaviour when compared to  $\pi^-$ ,  $K^-$  and  $\bar{p}$ .

18] predict collective flow expansion in proportion to particle mass, such as those exhibited by  $\pi^-$ ,  $K^-$  and  $\bar{p}$ . The centrality dependence of  $\langle p_T \rangle$  for the  $\phi$  meson shows a distinctive difference from that for the  $\pi^-$ ,  $K^-$  and  $\bar{p}$ . This may indicate that the evolution dynamics of the  $\phi$  meson is less sensitive to hadronic rescattering.

#### 4. Conclusions

We have presented results on  $\phi$  meson production at mid-rapidity in Au+Au and pp collisions at  $\sqrt{s_{NN}} = 200$  GeV. The spectrum in pp collisions is significantly different from that in Au+Au collisions. The spectra in Au+Au collisions weakly depend on the collision centralities. The extracted  $\phi$  yield is a linear function of the number of charged particles produced in the collision. The weak dependence of  $\phi \langle p_T \rangle$  on the centralities in Au+Au collisions is consistent with the expectation that  $\phi$  does not interact strongly with nonstrange hadronic matter.

#### Note(s)

a. E-mail: jgma@physics.ucla.edu

---

## References

1. P. Koch, B.Muller, J. Rafelski, *Phys. Rep.* **142** (1986) 167.
2. Rafelski et al., *Phys. Rev. Lett.* **48** (1982) 1066.
3. A. Shor, *Phys. Rev. Lett.* **54** (1985) 1122.
4. C.P. Singh, *Phys. Rev. Lett.* **56** (1986) 1750.
5. A. Bhattacharyya et al., *nucl-th/9602042*.
6. F. Klingl et al., *hep-ph/9709210*.
7. T. Hatsuda, T. Kunihiro, *Phys. Rep.* **247** (1994) 221.
8. C.M. Ko, P. Levai, X.J. Qiu, *Phys. Rev. C* **45** (1992) 1400.
9. B.A. Cole, *Nucl. Phys.* **A590** (1995) 179c.
10. C. Adler *et.al.*, *Phys. Rev. C* **65**, 041901(R) (2001).
11. STAR Collaboration, K.H. Ackermann et al., *Nucl. Phys.* **A661** (1999) 681c.
12. H. Wieman et al., *IEEE Trans. Nucl. Sci.* **44** (1997) 671.
13. D. L'Hote, *Nucl. Instrum. Meth.* **A337** (1994) 544.
14. D. Drijjar, H.G. Fishcher and T. Nakada, *Nucl. Instrum. Meth.* **A225** (1984) 367.
15. K. Hagiwara *et.al.*, *Phys. Rev. D* **66**, 010001 (2002).
16. C. Adler *et.al.*, *Phys. Rev. Lett.* **87**, 112303 (2001).
17. O. Barannik, F. Wang, STAR Collaboration, *QM2002 Proceedings*.
18. D. Teaney, J. Lauret, E.V. Shuryak *nucl-th/0110037*.